GSC Advanced Engineering and Technology

Cross Ref DOI: 10.30574/gscaet

Journal homepage: https://gsconlinepress.com/journals/gscaet/

(RESEARCH ARTICLE)

Check for updates

Amino acid-assisted synthesis and characterization of zero-Valente iron nanoparticles for research on the bio-interactions with yeast

Mažeika K [1], Pakštas V [1], Melvydas V [2] and Jagminas A [1,*]

[1] *State Research Institute Centre for Physical Sciences and Technology, Sauletekio ave. 3, LT-10257, Vilnius, Lithuania.*
[2] *Nature Research Center, Institute of Botany, Akademijos 2, LT-08412 Vilnius, Lithuania.*

GSC Advanced Engineering and Technology, 2022, 04(01), 001–011

Publication history: Received on 10 May 2022; revised on 13 June 2022; accepted on 15 June 2022

Article DOI: https://doi.org/10.30574/gscaet.2022.4.1.0043

Abstract

The wet synthesis of uniformly sized zero-Valente iron nanoparticles (NPs) for application in nanomedicine and biology is still a challenging because of magnetic interaction, oxidation and corrosion. In this study, various Fe-containing NPs were synthesized using amino acids as their size stabilizing agents to investigate their bio-interactions with *Metschnikowia* spp. yeast strains. For this, D-glutamic, DL-cysteine, DL-methionine, and taurine amino acids were tested. In this way, NPs in size from several to 40 nm, composed of a-Fe0, a-FeB, Fe2O3 and lepidocrocite, γ-FeOOH, were synthesized and characterized using X-ray diffraction and Mössbauer spectroscopy, and HRTEM investigations. The surprising influence of amino acid nature and DL-cysteine concentration on the NP size and composition has been revealed allowing fabrication of quite pure lepidocrocite as well as a-Fe0 NPs containing boron. As-synthesized NPs were cultivated in a YEPD growth media for research on the formation of insoluble red pigment pulcherrimin by several *Metschnikowia* spp. yeast strains. For comparison, the behavior of M. pulcherrima yeast with metallic iron plate and Fe0 NPs has been visualized.

Keywords: Zero-Valente Iron; Nanoparticles; Pulcherrimin Yeast; Self-Organization

1. Introduction

Numerous bacteria and yeast strains are capable produce pigments: insoluble, non-toxic, and biodegradable [1–3]. For these, they can be prospective in food industry, natural dyes and cosmetic products. Among others, the formation of pulcherrimin pigments by several bacteria such as *Bacilus circulans*, *subtilis*, *maceran*, *cereus*, etc. [4, 5] and yeast such as *Metschinikowia pulcherrima* and *Debraryomyces spp*. [6,7] have been reported. In the last case, water-insoluble red-colored pigment pulcherrimin is produced when yeast is growing in the media containing iron ions. It is characterized as a salt of pulcherriminic acid, namely 2,5-diisobutyl-3,6-dihydroxypyrazine-1,4-dioxide [8,9] secreted by microorganism. Because the formation reaction of pulcherrimin consumed iron ions the growth of other microbes should be prevented in such growth media [7]. Recently, this biofungicidal strategy could find various practical applications.

It has been suggested [6,7,10] that iron ions are consumed during yeast growth converting to pulcherrimin and precipitates of a red pigment. It is noticing that formation of insoluble pigment from the product secreted by yeast proceeds just when the concentration of Fe^{3+}-in-media species and secreted precursor by yeast exceeds the solubility product creating red concentric rings during cultivation on a solid agar media [11]. As reported, the content of red precipitates increased just up to critical concentration of Fe^{3+} ions (c_{Fe}) in the yeast growth media but the exact influence of c_{Fe} is still unclear implying on the bio-interaction variables. To the end and the best of our knowledge, the behavior

* Corresponding author: Jagminas A
State Research Institute Centre for Physical Sciences and Technology, Sauletekio ave. 3, LT-10257, Vilnius, Lithuania.

of yeasts capable produce red-colored insoluble pigment in the growth media containing Fe^0 nanoparticles (NPs) has not been studied yet. Therefore, this study was devoted to shed some light in the behavior of yeast with various Fe-containing NPs.

From the literature, the liquid-phase reduction of iron ions with borohydride is attributed to the most popular way for fabrication of Fe^0-based nanoparticles (NPs) for environment applications [12]. This method has been proposed by Glavee et al., as early as in 1995 [13]. The successful use of both ferric chloride, $FeCl_3$, and ferrous sulfate, $FeSO_4$, solutions have been reported [13-19]. Nurmi et al. [19] and Liu et al. [15] investigated the structure and size of nano-iron particles synthesized by this way indicating their irregular shapes in size from several to 100 nm. Similar results have been reported by other investigators [14,16,18]. The composition of iron NPs synthesized by borohydride reduction, however, is not clear resolved yet. It is assumed that iron NPs fabricated from the alkaline aqueous solutions by borohydride reduction are covered with polycrystalline Fe(III) oxide shell, driven by easy oxidation of Fe^0 [15,19,20]. Siskova et al. [21] reported that there are distinct differences in zero-Valente iron content in the NP formed by borohydride reduction of ferrous sulfate in the presence of some selected amino acids as mediators. For example, the presence of L-glutamic acid in the synthesis reactor promotes Fe^0 formation whereas DL-cysteine hindered it completely resulting just in ferric oxide formation. Besides, almost no effect of pH has been observed for DL-cysteine and L-arginine containing solutions. However, the influence of the tested amino acids on the size and shape of iron-containing NPs as well as on the shell composition have not been elucidated. The inclusions of boron and formation of *a*-FeB alloy have not been also analyzed assuming that ferric ions is reduced by the borohydride *via* reaction [22]:

$$4Fe^{3+} + 3BH_4^- + 9\ H_2O = 4Fe^0 + 3H_2BO_3^- + 12\ H^+ + 6\ H_2 \qquad (1)$$

However, the reduction of metal ions with borohydride at atmospheric pressure most often leads to the formation of amorphous metal borides since the temperature of aqueous solutions is not sufficient to trigger crystallization [23-26]. Note that the content of boron inclusions in the amorphous FeB can achieve 28 at.% [27]. Therefore, it was assumed that contamination of boron in the Fe^0 NPs can markedly influence yeast behavior and should be examined. Consequently, the first aim of the present work was to synthesize Fe NPs differing in the composition and size, biodegradable and non-toxic. As these, nano-scaled Fe^0 NPs mediated by several amino acids were synthesized, characterized, and tested.

2. Experimental Method

2.1. Chemicals

Agar was obtained from Reakhim, peptone and glucose – from AppliChem, yeast extract – from Liofilchem, DL-methionine (99.0%), L-glutamic (99.5 %), and taurine (99.5 %) were purchased from Sigma-Aldrich, whereas DL-cysteine (96 %) – from Raanal, Hungary. Used *Metschnikowia pulcherrima* yeast strain (M.P.) was obtained from the CBS-KNAW Fungal Biodiversity Center (Ultrecht, Netherlands). *Metschnikowia sinensis* (strains M4 and M6), and *M. shanxiensis* (M10) were isolated and identified as described in [28,29]. For NP synthesis pure $FeSO_4\ 7H_2O$ (99.5%) was obtained from Sigma-Aldrich and $NaBH_4$ as well as NaOH (both chemical pure) – from Russia.

2.2. Yeast growth and cultivation

The ability of yeast to secrete an insoluble pulcherrmin pigment was studied on two different growth media. YEPD media comprised of 10 g/L of yeast extract, 20 g/L peptone, 20 g/L glucose, 20 g/L agar, and various iron-containing NPs were dispersed in the 9 cm diameter-sized Petri dishes by ultra sound agitation during cool down from 70 °C to hardening temperature. Then, the pre-grown yeasts were spotted on YEPD layer, in height of ~5 mm, and allowed to grow for 1-30 days at 25 °C temperature. The content of iron in the tested media was determined using an inductively coupled plasma optical emission spectrometer Optima 7000 DV at wavelengths 238.204 and 239.562 nm after sample dissolution with HCl: HNO3:H2O (1:7:2) solution. All experiments were repeated at least 3 times. To estimate the extraction of NPs from the deeper agar layers, the yeast biomass was rinsed from the growth medium with distilled water.

2.3. Synthesis of zero-Valente iron NPs

The synthesis of iron NPs was conducted by $FeSO_4$ solution reduction with sodium borohydride as described previously in [21]. Briefly, 10 ml of aqueous 20 mmol L^{-1} $FeSO_4$ solution was quickly poured with 40 ml of cold (3-4 °C) 0.2 mol L^{-1} $NaBH_4$ solution and kept further 10 min under intense stirring. To obtain uniformly sized NPs several amino acids in concentration from 0.2 to 4.0 mmol L^{-1} were applied as NP growth mediators. The synthesized product was collected

by either magnetically separation or centrifugation at 7,500 rpm for 10 min, then washed with acetone (three times with 20 mL probes), and dried at 60 °C overnight.

2.4. Characterization

The morphology of as-grown products was investigated using a transmission electron microscope (TEM, model MORGAGNI 268) operated at an accelerating voltage of 72 keV. The NPs subjected to TEM observations were dispersed in ethanol and drop-cast onto the carbon-coated copper grid. Their average size was estimated from at least 150 species observed in the TEM images. High resolution transmission electron microscopy (HRTEM) studies were performed using a LIBRA 200 FE at an accelerating voltage of 200 keV.

X-ray powder diffraction experiments were performed on a D8 diffractometer (Bruker AXS, Germany), equipped with a Göbel mirror as a primary beam monochromator for CuK_{α} radiation. The average diameter (D) of crystallites comprised NPs was calculated from the broadening of the XRD peak intensity using the Debye-Scherer equation, $D = k\lambda/\beta\cos\theta$, where k is the Scherer factor (0.89), λ is the X-ray wavelength (0.154 nm) and β is the line broadening of a diffraction peak at angle θ [30].

Mössbauer spectra (MS) were collected in the transmission geometry from the spot of synthesized nanoparticles formed onto the shred of filter paper using Co^{57}(Rh) source. A closed cycle He cryostat (Advanced Research Systems, Inc.) was used for low temperature measurements. The hyperfine field B distributions and separate sextets or doublets were applied to fit the experimental spectra using WinNormos (Site, Dist) software distinguishing metallic α-Fe, amorphous Fe borides a-Fe-B, Fe_2O_3 , magnetite Fe_3O_4 and etc. At low temperature small area (1 %) is due to Fe in cryostat Be widows.

3. Results and discussion

3.1. Fabrication and characterization of iron nanoparticles

In this study, the use of amino acids as mediators of Fe^0 NP growth was inspired by the facts that these NPs are stable for months, eco-friendly [21,31], and expected could be able for the synthesis of insoluble pigment - pulcherrimin by *Metschinikowia* spp. yeasts. However, it was found herein that the kind of amino acid and its concentration markedly influenced the size and composition of NPs synthesized by borohydride reduction of Fe(II) solutions. In the case of taurine usage from 0.4 to 4.0 mmol L^{-1}, just amorphous species were obtained, whereas the products synthesized with D,L-cysteine markedly depends on the concentration of this additive. In the case of glutamic acid, mainly zero-Valente Fe species were formed corroborating to the report of [21]. Shown in figure 1 are room (A) and 11 K (B) temperature Mössbauer spectra (MS) of NPs grown in the solutions containing either D,L-cysteine or glutamine amino acid, as growth stabilizer. The analysis of these MS showed that NPs mediated by a small content of D,L-cysteine, e.g. 0.2-0.33 mmol L^{-1}, labeled as A-a and A-b, (Table 1) are composed of metallic a-Fe, amorphous iron boride and just 12-16 % of Fe(III) oxides for which (Figure 1 B-a, Table 1) the average hyperfine field at 11 K is considerably lower than that of well crystallised Fe oxides [32], therefore, this part of spectrum should be attributed to amorphous Fe(III) oxide [33]. The largest amount of iron in these samples is in amorphous iron boride form which is identified according to isomer shift which values are intermediate between these of a-Fe^0 and Fe(III) oxides [34,35]. Note that hyperfine field distribution attributed to iron borides ranges within 5-45 T at room temperature. In our case, the average hyperfine field of as-synthesized NPs is 23- 24 T. Besides, the sextets of Fe_3B and Fe_2B inter-metallic compounds having hyperfine fields of 28.6, 26.7, 23.8, and 22.3 T at room temperature [35] were not distinguishable in the broad part of spectra attributable to amorphous iron boride. For these our samples, the presence of metallic

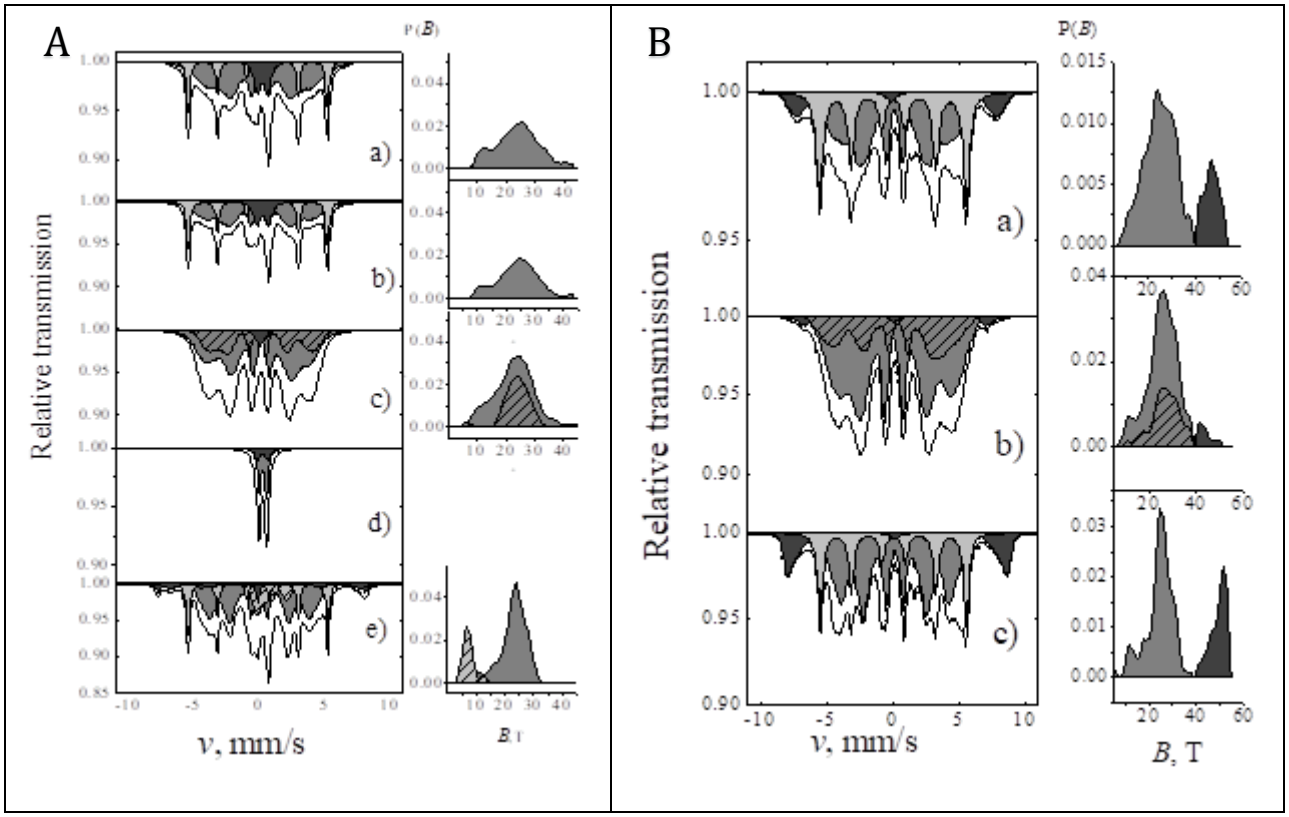

Figure 1 Room temperature (A) and cryogenic temperature (B) Mössbauer spectra of NPs synthesized via reduction of 20 mmol L-1 FeSO4 with 0.24 mol L-1 NaBH4. The solutions contained additionally 0.24 (A-a, B-a), 0.33 (A-b) either 3.0 mmol L-1 (A-d) of cysteine, or 4.0 (A-c, B-b) either 0.4 (A-e, B-c) mmol L-1 of glutamic amino acid. In the right sides – the corresponding hyperfine field distributions P (B)

α-Fe^0 is visible in the spectra as characteristic sextet having hyperfine field of 33.1 T and isomer shift $\delta \cong 0$ mm/s relatively to α-Fe^0 of calibration foil at room temperature. The α-Fe^0 content reaches up to third of iron in the samples.

Similar composition was determined for NPs grown in the same Fe(II) and borohydride solution containing 0.4 mmol L^{-1} of glutamic amino acid (A-e, B-c sample), although these NPs contained some larger content of iron oxides, namely 0-30 % in which Fe is mixed valence Fe(II, III) according to presence of magnetite subspectra and the isomer shift value δ=0.775±0.004 mm/s of hyperfine distribution within 3-15 T [32]. At a low temperature, these sub-spectra transform to the magnetically split area of spectra described by hyperfine field distribution within 40-55 T (Figure 1B right) having an average hyperfine field of 49 T (Table 1).

However, if significantly higher amount of glutamic acid is used (sample A-c and B-b) as-grown NPs are composed almost entirely of iron borides except probable small amount of amorphous Fe oxide distinguishable at low temperature (B-b spectrum) (Table 1). Note that to fit to this MS at least two hyperfine field distributions having different quadrupole shifts should be used. Different quadrupole shifts are because of disordering the NPs being in an amorphous state which induces variations of electric field gradient tensor and magnetic order at the Fe sites.

The composition of NPs obtained in the solutions containing a small amount of cysteine not satisfied with [21] that cysteine completely hindered zero-Valente iron growth by Fe(II) borohydride reduction approach. We found, however, that this is true just in the case when a significantly higher content of cysteine is applied (Figure 1A-d). Judging from the room temperature MS (Fig. 1A-d) and XRD (Figure 3c) NPs as-formed in the more concentrated cysteine solutions are very small, brown-colored and composed mainly of Fe(III) oxide/hydroxide, *α*-FeOOH.

Table 1 Parameters of Mössbauer spectra: relative contribution to subspectra, *A*, isomer shift relatively to *α*-Fe^0 at room temperature, *δ*, quadrupole shift (splitting for doublets), $2\varepsilon(\Delta)$, and hyperfine field, *B*. Average values are shown in the case of hyperfine field distributions, Sample denotes concentration of amino acid

Sample	T, K	*A*, %	*δ*, mm/s	$2\varepsilon(\Delta)$, mm/s	*B*, T	Phase
A-a	296	21	0.001±0.001	-0.001±0.002	33.09±0.01	*α*-Fe
		12	0.359±0.003	0.755±0.007	-	Fe_2O_3
		67	0.136±0.003	-0.07±0.005	24.01*	a-Fe-B
B-a	11	30	0.131±0.009	-0.03±0.01	34.38±0.05	α-Fe
		16	0.379±0.018	0.01±0.04	46.68*	a-Fe_2O_3
		53	0.248±0.011	0.02±0.02	24.47*	a-Fe-B
		1	0.244**	-	-	Fe in Be w.
A-b	296	28	0.001±0.001	-0.003±0.002	33.11±0.01	α-Fe
		13	0.381±0.004	0.87±0.01	-	Fe_2O_3
		59	0.101±0.005	-0.023±0.008	23.99*	a-Fe-B
A-c	296	66	0.114±0.005	-0.304±0.005	22.74*	a-Fe-B
		30	0.114***	0.247±0.005	23.68*	a-Fe-B
		4	0.146±0.008	-	-	a-Fe-B
B-b	11	69	0.231±0.011	0.12±0.01	25.42*	a-Fe-B
		26	0.231***	-0.59±0.03	26.85*	a-Fe-B
		4	0.54±0.02	-0.55±0.04	44.25*	*α*-Fe_2O_3
		1	0.244**	-	-	Fe in Be w.
A-d	296	60	0.380±0.001	0.538±0.004	-	Fe(III)
		40	0.352±0.005	0.77±0.04	-	Fe(III)
A-e	296	19	0.001±0.001	0.003±0.002	33.20±0.01	*α*-Fe
		51	0.109±0.003	0.014±0.004	23.05*	*α*-Fe-B
		14	0.775±0.004	0.67±0.01	7.33*	Fe(II,III) o.
		4	0.441±0.003	0.895±0.007	-	Fe(III) oxide
		5	0.282±0.008	0.016±0.016	49.27±0.05	Fe_3O_4
		7	0.55±0.02	0**	45.11±0.17	Fe_3O_4
B-c	11	23	0.144±0.002	-0.023±0.005	34.25±0.02	*α*-Fe
		53	0.254±0.003	0.012±0.006	24.31*	a-Fe-B
		23	0.439±0.004	0.019±0.009	49.19*	Fe(II,III) o.
		1	0.244**	-	-	Fe in Be w.

*average of hyperfine field distribution; **fixed; ***equal

The characterization of NPs synthesized *via* reduction of Fe (II) solutions containing methionine with borohydride is highlighted in figure 2. From the calculations of nanocrystallites size by Sherrer approach using experimental XRD patterns (Figure 2A), the methionine mediated iron-based NPs are extremely small and not exceed 2 nm. According to the MS parameters (Table 2) these NPs are composed almost entirely of iron borides except the small amount of amorphous Fe oxide, capable to be distinguished just at cryogenic temperature. To fit better their room temperature MS, at least two hyperfine field distributions having different quadrupole shifts should be used. Note that different

quadrupole shifts can be explained by atom disordering in amorphous state thereby inducing variations of electric field gradient tensor and magnetic order at Fe sites. We note that the composition of methionine mediated NPs is similar to glutamic acid- c

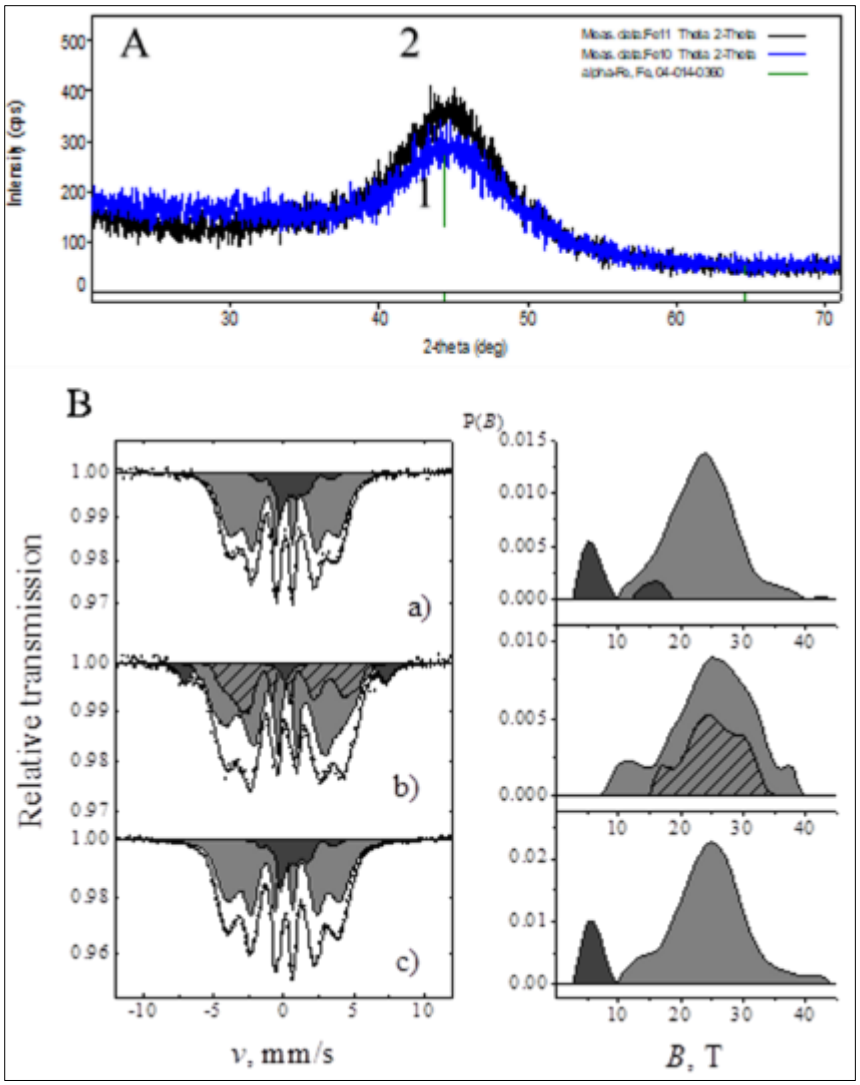

Figure 2 XRD patterns (A) and Mössbauer spectra (B) of iron NPs synthesized by methionine acid assisted synthesis from Fe^{2+} and sodium borohydride solutions during 10 min. The cold solutions containing 3.0 mmol L^{-1}(A-1, B-a and B-b) or 0.4 mmol L^{-1} (A-2, B-c) of methionine were used. MS were recorded at an ambient (B-a and B-c) and cryogenic, ca. 11 K, (B-b) temperatures. In the right – hyperfine field distributions P (*B*) of corresponding samples

Stabilized NPs (Figure 2A-c) although the shape of their MS in the central part is slightly different. Probably in this case, a small contribution of amorphous oxides contain Fe (II), according to isomer shift values (Table 2).

XRD patterns of NPs synthesized in the solutions without and containing D,L-cysteine amino acid are shown in figure 3. From these, NPs formed in the additive-free solution are composed mainly of zero-Valente iron, Fe^0. The contents of iron boride, Fe_3B, and iron hydroxide, $Fe(OH)_2$ inserted in these NPs are low and the size of Fe-containing crystallites varied within several to 100 nm (Figure 3d).

Table 2 The parameters of Mössbauer spectra presented in figure 2B: Sample denotes methionine concentration, A - the relative contribution of subspectra, δ – isomer shift relatively to a-Fe at room temperature, $2\varepsilon(\Delta)$– quadrupole shift (splitting for doublets) and B – hyperfine field. Average values are shown in case of hyperfine field distributions

Sample	T, K	*A*, %	*δ*, mm/s	$2\varepsilon(\Delta)$, mm/s	*B*, T	Phase
B-a	296	85	0.170±0.005	-0.018±0.008	23.57*	a-Fe-B
		15	0.622±0.006	0.28±0.02	8.31*	a-Fe_2O_3
B-b	11	61	0.226±0.007	-0.312±0.015	24.92*	a-Fe-B
		26	0.226***	0.59±0.03	25.12*	a-Fe-B
		11	0.24±0.03	0**	44.4±0.2	a-Fe_2O_3
		2	0.244**	-	-	Fe in Be w.
B-c	296	85	0.121±0.002	-0.025±0.003	24.72*	a-Fe-B
		15	0.689±0.005	0.375±0.006	8.14*	a-Fe_2O_3

*average of hyperfine field distribution; **fixed; ***equal

XRD patterns of species formed by Fe(II) ions reduction in the presence of 2 mmol L^{-1} glutamic acid indicated on the formation of mixture from the Fe^0 (31 %), magnetite, Fe_3O_4 (32 %), $Fe(OH)_2$ (9 %), goethite, FeO(OH) (14 %), and chukanovite, $Fe_2(CO_3)(OH)_2$, crystallites differing in size. However, according to the Mössbauer spectra parameters (Table 1, A-e sample) significantly higher contents of zero-Valente Fe^0 and FeB species are formed. The largest crystallites in size of 38-40 nm possessed Fe^0 whereas the size of oxide fractions varied from 2.5 (hydroxide) to 8 nm.

In contrast to Siskova et al. report [21] indicating that DL-cysteine completely hindered zero-Valente iron growth by Fe(II) borohydride reduction approach we found by XRD tests that low concentrations of DL-cysteine acid applied during the synthesis still result in the growth of pure

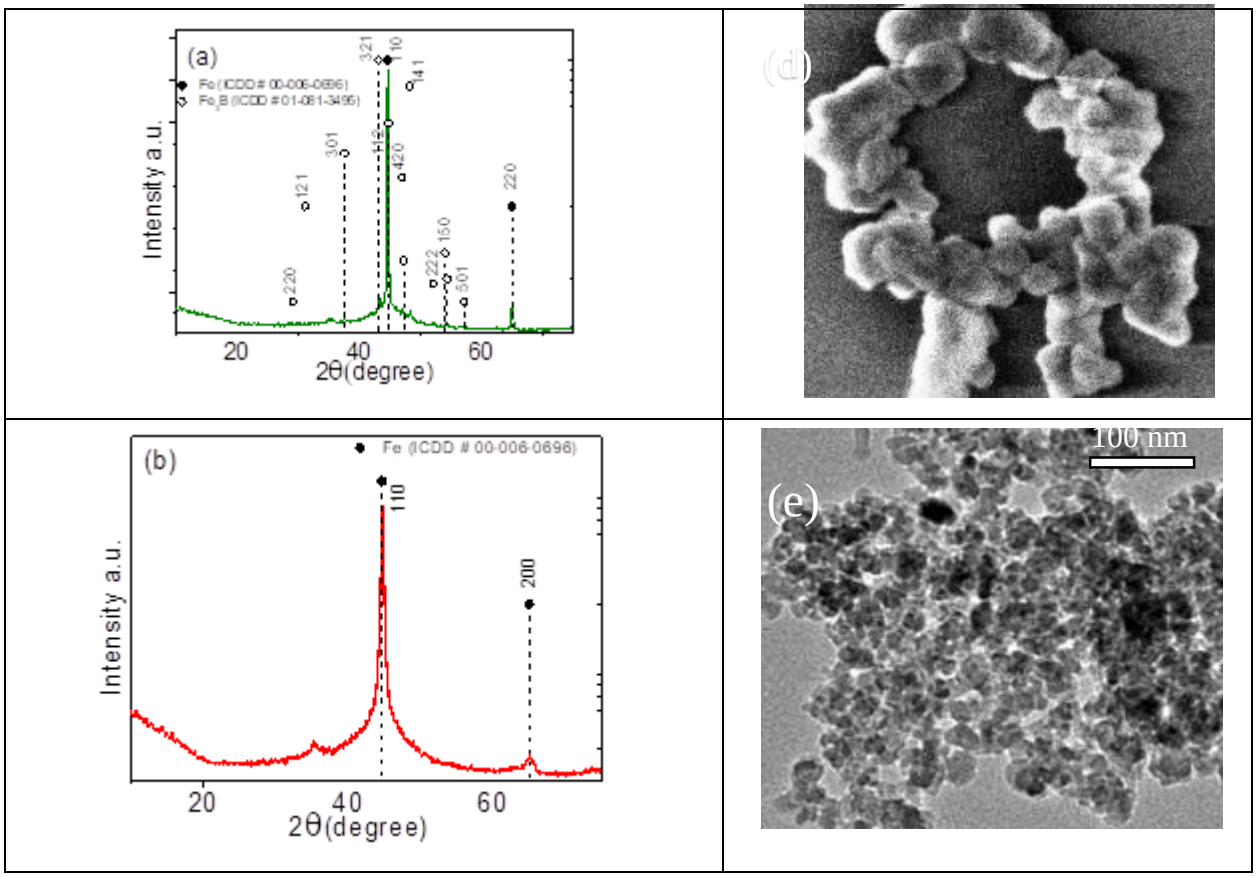

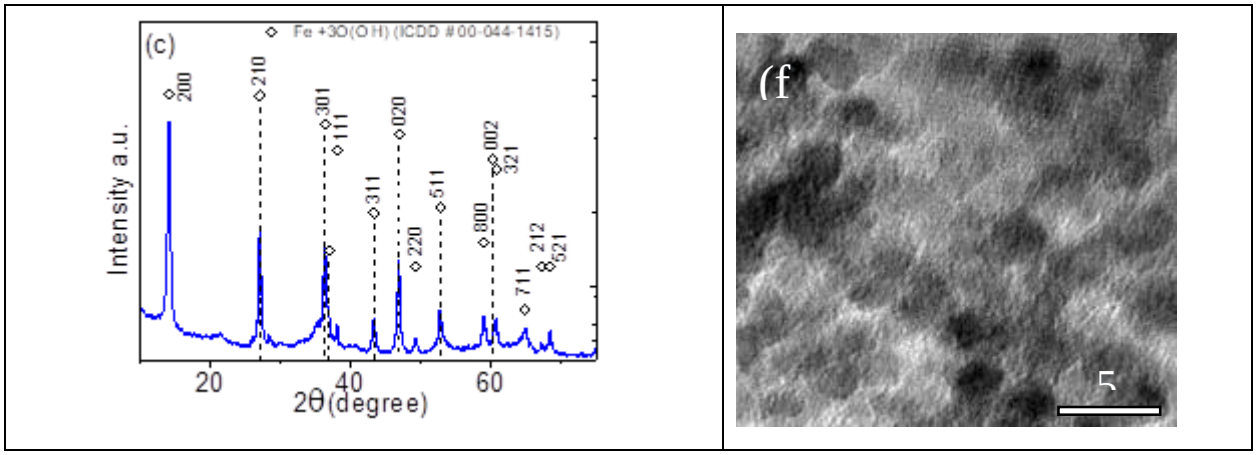

Figure 3 XRD patterns of NPs synthesized by 20 mmol L-1 Fe2SO4 reduction with 0.24 mol L-1 borohydride in the absence (a) and presence of 0.24 (b) and 3.0 mmol L-1 (c) D,L-cysteine. In the right side, the SEM (d, e) and HRTEM (f) images of these products are shown

Fe^0 NPs (Figure 3b). Besides, significantly smaller and uniformly sized NPs can be obtained compared to the synthesis products in the additive free solutions (Figure 3e). However, if significantly higher concentration of D,L-cysteine was applied, the synthesized product is composed just of iron(III) oxide/ hydroxide (Figure 3c) in the form of ultra-small and nonmagnetic NPs (Figure 3f) as has been reported [21].

3.2. Formation of pulcherrimin pigment by Metschnikowia spp. yeast cultivated with iron-containing Nps

From the previous reports [11,29], a red-brown coloured insoluble pigment pulcherrimin is synthesized by the strains of *Metschnikowia* spp. yeast in the YEPD growth media containing iron ions. Worth noticing that formed biomass accumulate iron in chlamydospores preventing growth of other microorganisms [28]. To the best of our knowledge, the influence of iron-containing NPs on the formation of antimicrobial pulcherrimin pigment is not clear yet. Therefore, several Fe-containing NPs synthesized herein were used to estimate their influence on the formation of pulcherrimin. Highly active *Metschnikowia* yeast strains, capable secrete the pulcherriminic acid, namely M4 (*M. sinensis*), M6 (*M. sinensis*), M10 (*M. shanxiensis*), and M.P. (*M. pulcherrima*) were tested using the same experimental approach as in Melvydas, et al. [11] study. Briefly, *Metschnikowia* spp. yeast strains were inoculated at 25 °C by dots and streaks onto the YEPD growth media layer containing Fe NPs (grown in Petri dishes for 6 days, ~5 mm thick). The colour of formed biomass was observed for 30 days. The content of NPs was about 200 mg/kg (10 mg of NPs distributed in 50 mL).

The images of tested four *Metschnikowia* spp. strains in the dot and streak sites after explosion onto the growth media with ultra-small α-Fe^0 NPs and γ-FeOOH (lepidocrocite) NPs for three and 5 days are depicted in Figure 4 left and right parts, respectively. From the reddish-brown colours of inoculated dots and strains it is obvious that all tested strains produce pucherrimin pigment when YEPD growth media contained α-Fe^0 NPs. Most intense colouring was obtained for *M. sinensis* yeast M6 strain. Besides, just for this strain light brown coloured sites of removed biomass are viewed implying on the formation of pigment even in deeper agar layers.

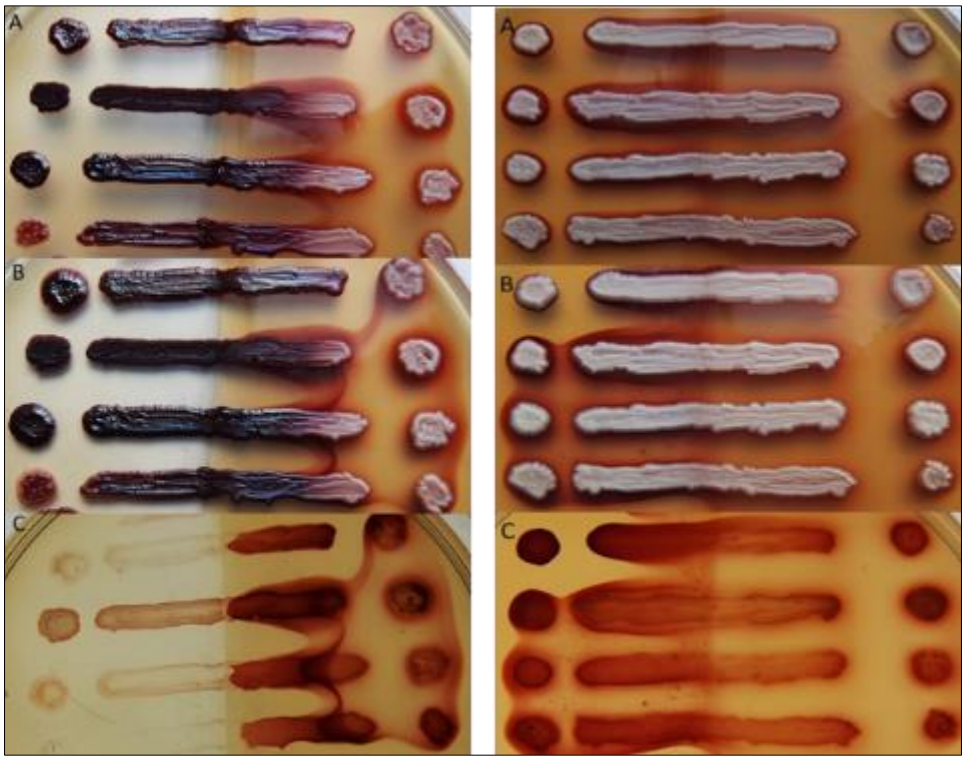

Figure 4 The colors of *Metschnikowia* spp. yeast strains: M4, M6, M10, and M.P. (from the top side, respectively), grown for 7 days at 25 °C and cultivated with ultra small *a*-Fe^0 NPs (in the left panel) and FeOOH NPs (in the right panel) for three (A) and 5 (B,C) days before (B) and after (C) rinse. *a*-Fe^0 NPs were synthesized with methionine (2 mmoL/L) amino acid

Such intensity colouring of biomass products have been obtained on the yeast growth media cultivated with high content of Fe salt [29]. Quite similar results were also obtained in the case of *a*-FeB NPs cultivation in the yeast growth media implying that alloying of iron NPS with boron not safeguard from NPs dissolution by pulcherminic acid and synthesis of red-brown biomass.

Peculiarities of pucherrimin biomass formation in the yeast growth media with FeOOH NPs illustrate figure 4 right panel. In contrast to *a*-Fe^0 and *a*-FeB NPs, red-brown coloured pucherrimin pigment seems not formed in the YEPD growth media with lepidocrocite NPs for all tested *Metschnikowia* spp. yeast strains. In this case, the color of biomass after 5 days growth is white for all tested strains. When white biomass was removed from the yeast growth medium surface by washing, the light-brown color of remained dots and streaks testified precipitation of pulcherrimin in the some depth of agar layer. To study the accumulation peculiarities of iron-based NPs in chlamydospores sequestrating iron from the growth medium and the mechanism of biochemical processes the further studies are required.

4. Conclusion

D,L-cysteine, D,L-methionine, L-glutamic, and taurine amino acids were used for wet synthesis of iron-based NPs. In this way, NPs in size of from several to 40 nm composed of *a*-Fe^0, *a*-FeB, Fe_2O_3, and γ-FeOOH (lepidocrocite) were synthesized and characterized by X-ray and Mössbauer spectroscopy, and HRTEM. The D,L-cysteine concentration dependent formation of pure iron and iron oxide NPs estimated for the first time. *a*-FeB NPs were grown by reduction of Fe^{2+} with borohydride. These NPs were cultivated in the typical yeast growth media and investigated on the formation of red-brown colored pucherrimin pigment by several *Metschinikowia* spp. yeast strains. High activity of ultra-small *a*-Fe^0 NPs as well as *a*-FeB NPs was estimated for this pigment formation.

Compliance with ethical standards

Acknowledgments

The authors are sincerely grateful to Dr. Marija Kurtinaitiene for nanoparticles synthesis.

Disclosure of conflict of interest

The authors declare that they have no known competing financial interests or personal relationships that could have appeared to influence the work reported in this paper.

References

[1] Venil CK, Zakaria ZA and Ahmad WA. (2013). Bacterial pigments and their applications, Process Biochemistry, 48, 1065–1079.

[2] R. Panesar R, Kaur S and Panesar PS, (2015). Production of microbial pigments utilizing agro-industrial waste: a review. Current Opinion in Food Science, 1, 70–76.

[3] Tuli HS, Chaudhary P, Beniwal V and Sharma AK. (2015) Microbial pigments as natural color sources: current trends and future perspectives. Journal of Food Science Technology, 52, 4669–4678.

[4] Kupfer DG, Uffen RL and Canale-Parola E. (1967). The role of iron and molecular oxygen in pulcherrimin synthesis by bacteria. Archives of Mikrobiology, 56, 9–21.

[5] Uffen RL and Canale-Parola E. (1972). Synthesis of pulcherriminic acid by Bacilus subtilis. Journal of Bacteriology, 111, 86–93.

[6] Sipiczki M. (2006). Metschnikowia strains isolated from botrytized grapes antagonize fungal and bacterial growth by iron depletion. Applied Environmental Microbiology, 72, 6716–6724.

[7] Turkel S and Ener B. (2009). Isolation and characterization of new Metschnikowia pulcherrima strains as producers of the antimicrobial pigment pulcherrimin. Z. Naturforsch. C, 64, 405–410.

[8] Kluyver AJ, Van der Walt JP and Van Triet AJ. (1953). Pulcherrimin the pigment of Candida pulcherrima. Proc. Natl. Acad. Sci. U.S.A., 39, 583–593.

[9] Cook AH and Slater CA. (1956) The structure of pulcherrimin. Journal of Chemical Society, 4133–4135.

[10] Saravanakumar D, Ciavorella A, Spadaro D, et al. (2008). Metschnikowia pulcherrima strain MACH1 outcompetes Botrytis cinerea, Alternaria alternata and Penicillium expansum in apples through iron depletion. Postharvest Biological Technology, 49, 121–128.

[11] Melvydas V, Staneviciene R, Balynaite A and Vaiciuniene J. (2016). Formation of self-organized periodic patterns around yeasts secreting a precursor of a red pigment. Microbiological Research, 193, 87-93.

[12] Li L, Fan M, Brown RC, Van Leeuwen JH, et al. (2010). Synthesis, properties, and environmental applications of nanoscale iron-based materials: A review. Crit. Rev. Environmental Science Technology, 36, 405-431.

[13] Glavee GN, Klabunde KJ, Sorensen C and Hadjipanayis GC. (1995). Chemistry of borohydride reduction of iron(II) and iron(III) ions in aqueous and nonaqueous media. Formation of nanoscale Fe, FeB and Fe2B powders, Inorganic Chemistry, 34, 28–33.

[14] Zhang WX. (2003). Nanoscale iron particles for environmental remediation: an overview. Journal Nanoparticle Research, 5, 323–332.

[15] Liu YQ, Majettich SA, Tilton RD, Sholl DS and Lowry GV. (2005). TCE dechlorination rates, pathways, and efficiency of nanoscale iron particles with different properties. Environmental Science Technology, 39, 1338–1343.

[16] Kanel SR, Manning B, Charlet L and Choi H. (2005). Removal of arsenic (III) from groundwater by nanoscale zero-Valente iron', Environmental Science Technology, 39, 1291–1296.

[17] Elliott DW and Zhang WX. (2001). Field assessment of nanoscale bimetallic particles for ground water treatment. Environmental Science Technology, 35, 4922–4926.

[18] Choe S, Chang YY, Hwang KY and Khim J. (2000). Kinetics of reductive denitrification by nanoscale zero-valent iron. Chemosphere, 41, 1307–1312.

[19] Nurmi JT, Tratnyek PG, Sarathy V, et al. (2005). Characterization and properties of metallic iron nanoparticles: Spectroscopy, electrochemistry, and kinetics. Environmental Science Technology, 39, 1221–1227.

[20] Uegami M, Kawano J, Kakuya K, Okita T and Okinaka K. (2004). Iron composite particles for purifying soil or groundwater. Eur. Patent Appl., No EP1283519A1.

[21] Siskova KM, Straska J, Krizek M, et al. (2013). Formation of zero-valent iron nanoparticles mediated by amino acids. Procedia Environmental Science, 18, 809–817.

[22] Zhang WX, Wang CB and Lien HL. (1998). Treatment of chlorinated organic contaminants with nanoscale bimetallic particles. Catalysis Today, 40, 387–392.

[23] Carenco S, Portehauult D, Boissiere C and Mezailles N. (2013). Nanoscaled borides and phosphides: Recent developments and prospectives. Chemical Reviews, 113, 7981–8065.

[24] Wells S, Charles SW, Mørup S, et al. (1989). Journal of Physics: Condensed. Materials, 1, 8199–8206.

[25] Shen J, Li, Z, Yan Q and Chen Y. (1993). Reaction of bivalent metal ions with borohydride in aqueous solution for the preparation of ultrafine amorphous alloy particles. Journal of Physical Chemistry, 97, 8504–8511.

[26] Saida J, Inoue A and Masumoto T. (1991). The effect of reaction condition on composition and properties of ultrafine amorphous powders in (Fe, Co, Ni)-b systems prepared by chemical reduction. Metallurgical and Materials Transaction A, vol. 22, pp. 2125–2132, 1991.

[27] Linderoth S and Mørup SJ. (1990). Chemically prepared amorphous Fe-B particles: Influence of pH on the composition. Journal of Applied Physics, 67, 4472–4474.

[28] Melvydas V, Svediene J, Skridlaite G, et al. (2020). In vitro inhibition of Saccharomyces cerevisiae frowth by Metschnikowia spp. Triggered by fast removal of iron via two ways. Brazil Journal of Microbiology, 51, 1953–1964.

[29] Maźeika K, Šiliauskas L, Skridlaitė G, et al. (2021). Features of iron accumulation at high concentration in pulcherrimin-producing Metschnikowia yeast biomass. Journal of Biological Inorganic Chemistry, 26, 299–311.

[30] Guinier A, Lorrain P and Lorrain DS-M. (1963). X-Ray Diffraction : In Crystals, Imperfect Crystals and Amorphous Bodies. Freeman, W.H. & Co.: San Francisco, CA, USA.

[31] Marinescu G, Patron L, Culita DC et al. (2006). Synthesis of magnetite nanoparticles in the presence of aminoacids. Journal of Nanoparticle Research, 8, 1045–1051.

[32] Oh SJ, Cook DC and Townsend HE. (1998). Characterization of iron oxides commonly formed as corrosion products on steel. Hyperfine Interactions, 112, 59–65.

[33] Machala L, Zboril R and Gedanken A. (2007). Amorphous iron(III) oxide–A review. Journal of Physical Chemistry B, 111, 4003-4018.

[34] Hoving W and Van der Woude F. (1986). Extracting structural information from Mossbauer isomer shift data in amorphous iron-boron alloys. Hyperfine Interactions, 27, 433-436.

[35] Jiang J, Zhao F, Gao P, Dezsi L andGonser U. (1990). Crystallization of Fe-B amorphous alloy powders produced by chemical reduction. Hyperfine Interactions, 55, 981–986.